Journal of Scientific & Industrial Research
Vol. 83, October 2024, pp. 1066-1074
DOI: 10.56042/jsir.v83i10.10112

Identification of Clay mineral deposits in the South-Eastern region of Uttar Pradesh, India, using Remote Sensing

Debiprasad Karmakar[1]* & Swapankumar Ghosh[2]*

CSIR-Central Glass & Ceramic Research Institute, Khurja Centre, India

[1]CSIR-Recruitment and Assessment Board, CSIR Complex, Library Avenue, New Delhi-110 012

[2]Presently working at Department of Chemistry, West Bengal State University, Berunanpukuria, Kolkata-700 126

Received 02 April 2024; revised 09 July 2024; accepted 19 September 2024

Finding new mineral deposits is very important for the economic growth of a country. Recent advancements have made exploration of minerals very easy with the help of satellite imagery. Several inaccessible areas can be explored for the presence of deposits. The present article focuses on the analysis of the Landsat imagery of 2018 using datasets from the Landsat 8 (OLI/TIRS) satellite. The unsupervised classification with maximum likelihood algorithm is applied to bring out probable classes. It is found that the major classes are wasteland and forest followed by vegetation, water body, sand, built-up, limestone, kaolin and rocky land. The main objective is to find the kaolin rich zones which accounted for ~1.08% of the study area. To validate the findings, field survey have been carried out, 15 clay samples are collected from the study area in Ramgarh-Naudiha region of Sonbhadra district and have been characterised for mineral content. The mined mineral is fine-grained, off-white, siliceous, ball clay which can be beneficiated to make it acceptable to Indian ceramic industries. The remote sensing study is useful in identifying clay mineral deposits in the study area in Sonbhadra district and brightens the hope of findings pristine mineral deposits in the other parts of the country also.

Keywords: Remote sensing, Landsat, Unsupervised classification, Field survey, Clay

Introduction

Traditionally, field observations from routine ground survey investigations were used to create geological maps. There are some inevitable mistakes and flaws as a result of the meticulous mapping and detail extrapolation used in these maps. The emergence of Remote Sensing (RS) and Geographic Informatic System (GIS) operations has led to ongoing modifications to mapping related procedures. These days, remote sensing methods are crucial to mapping initiatives.[1] Remote sensing data has many user friendly benefits e.g., the acquisition of several consecutive data sets, broad area coverage, cost data, precise data, and a sizable information repository.[2] Geologists have concentrated on worldwide experiences in a number of earth science domains, including environmental, mineral ore, and hydrocarbon exploration, using data gathered from remote sensing.[3] An excellent synoptic perspective is provided by remote sensing, which is not possible with the majority of other geophysical prospecting techniques. Another benefit is that it provides an integrated and regional view of the connections between different terrain characteristics.

China clay or kaolin is the name given to the minerals that are discovered to be abundant in kaolinite. Worldwide, secondary occurrences of Indian kaolinite, a common 1:1 dioctahedral phyllosilicate (clay) mineral can be found. It is an affordable, naturally occurring geomaterial with a wide range of qualities that make it ideal for a variety of applications in the fields of ceramic industry, agriculture, civil engineering, environment, and health care.[4,5] The kaolinite content and degree of structural disorder, along with any accompanying quartz and heavy metal impurities like Fe-Ti minerals, are the primary factors that determine the grade and quality of raw kaolin deposits for industrial applications. Kaolin formation, by natural weathering and transit after its creation from the rock source, often have an impact on its mineralogy and chemistry. The source of the clay can be determined largely by the mineralogy, texture, and geochemical properties of the deposit.[6] A crucial step in the natural creation of clay minerals such as kaolinite, smectite, and illite is argillic alteration. While some of these transformations may occur under atmospheric

*Author for Correspondence
E-mail: skghoshwb@gmail.com, dpkcgcri@gmail.com

settings, this is often a low temperature event.[7] This in turn has a significant impact on the physicochemical qualities of the kaolinitic clays, including their colour, opacity and whiteness, compactness, plasticity, and rheology.[8]

Since the latter decades of the 20th century, spectrophotometric analyses in the 400–700 nm wavelength range have shown to be a useful technique for detecting the mineralogical quality of kaolin deposits, ore:waste ratio determination, or other geological parameters.[9] China clay and associated minerals can easily be detected from their diagnostic spectral fingerprints in the 100–2500 nm range of the electromagnetic spectrum of which visible and near infrared (VNIR) has 350–2500 nm wave length and shortwave infrared SWIR has 1000–2500 nm wave length.[10–13] For detecting clay minerals to upto 1%, SWIR reflectance spectroscopy is very accurate. Structural order-disorder in kaolin can be evaluated from the equation,

$$14\text{Sp Index} = A - B/A,$$

where, A/2 and B/2 indicate the depths of the absorption features centred at ~1400 nm on the clay spectra. Any shift in absorption feature is indicative of variations in composition and crystal structure in the clay minerals.[14-16]

According to certain reports, the physical characteristics of soil, such as moisture content, organic matter, surface mineralogy, and particle size, all affect its reflectance spectrum.[17] Programmes e.g., Landsat-5 Thematic Mapper (TM), Landsat-7 Enhanced TM Plus, Landsat-8 Operational Land Imager (OLI), ASTER as well as Moderate Resolution Imaging Spectroradiometer (MODIS) could use remote sensing data to create clay, and other mineral distribution maps.[18,19]

It should be noted that the depth component of remote sensing data is a significant barrier for the exploration of minerals. A few micrometer in the VNIR, a few centimetre in the TIR, and a few metre (in hyper– and dry climates) in the microwave range are the deep penetrations of remote sensing data. An interpreter of a deposit must instead rely on indirect indicators, such as the general geologic setting, alteration zones, associated rocks, structures, lineaments, oxidation products, morphology, drainage network, and vegetation pattern, as it is challenging to directly identify the mineralogy of a deposit based only on remote sensing data. From this angle, it is anticipated that multispectral and hyperspectral sensors which are capable of defining mineralogy will contribute more to the field of mineral exploration by aiding in the identification of ore minerals and other pathfinders. An increasing number of operational exploration models based on GIS technology are incorporating the results, as it is important for mineral exploration.[20]

The mineral prospective map was successfully generated using Landsat 8 imagery, and was categoried as most, somewhat, and least suited for economic mineralisation potential.[21] The report concluded that, in contrast to conventional geophysical methods, geospatial techniques are less costly and time-consuming in finding mineral potential zones. OLI, Thermal Infrared Sensor (TIRS), and Landsat 8 data have been utilised for geological mapping and mineral exploration in north-central Sudan. Image processing techniques were applied to the Landsat operating imager to indicate the existence of alteration zones that are conducive to gold mineralisation using ArcGIS and processed numerical data using ERDAS Imaging. Combined GIS and remote sensing data were reported to enhance mining extraction in South Australia's Gawler ranges.[21] Such investigations are able to distinguish among epithermal silver mineralisation, porphyry copper, and gold. Altered mineralogy detection was achieved by airborne hyperspectral imagery and was able to isolate topographic features in close proximity to a possible porphyry copper mineralisation from chlorite alteration manifested at the surface prior to mineralisation.[21]

Traditional exploration methods such as geophysics and geochemical analysis are expensive, time-consuming, and have a limited geographic reach, and to the best of our knowledge, no systematic attempts have been documented to employ remote sensing techniques to find new clay deposit areas for industrial exploitation in northern India. This study was conducted in the Ramgarh-Naudiha region of the Sonbhadra district in Uttar Pradesh to determine the sites of likely clay zones based on our optical interpretation utilising Remote Sensing technique and then verifying the same by field survey. The research area's new clay zone sources have been discovered as a result of this investigation. Compared to other clay minerals, kaolinites typically have less complex fingerprint absorption features, which makes them an excellent choice for beginners to start with the clay spectra with morphological changes in the presence of other minerals.[9]

Materials and Methods

Study area and geologic setting

The location map of the study area in the Ramgarh-Naudiha region of Sonbhadra district is shown (Fig. 1). In terms of area, it is the second district and lies in the extreme south-east of the state. It is surrounded by Madhya Pradesh in the west, Chhattishgarh in the south, Jharkhand in the south-east and Bihar to the north-east.

Robertsganj town is the district headquarter. Sonbhadra is rich in minerals like, bauxite, limestone, coal, gold etc. It is called the "Energy Capital of India" because there are multiple power plants in the district. The study area lies on the south of Son river flowing from west to east near Ramgarh-Naudiha block (Latitude 24°28'N to 24°23'N, Longitude 83°12'E to 83°24'E).[8,22]

Satellite Data

The satellite images of Landsat 5 and 8 were used in this study. The acquired images in Geo-Tiff format were geo-referenced in the World Geodetic System (WGS84) datum, and projected in the Geographic and zone 44 N of UTM. While selecting satellite images, the absence of cloud cover and having no precipitation during two days prior the satellite's passage was considered (Table 1). In order to provide the training and test data for image classification and accuracy assessment of extracted maps, Landsat false colour composite was considered.

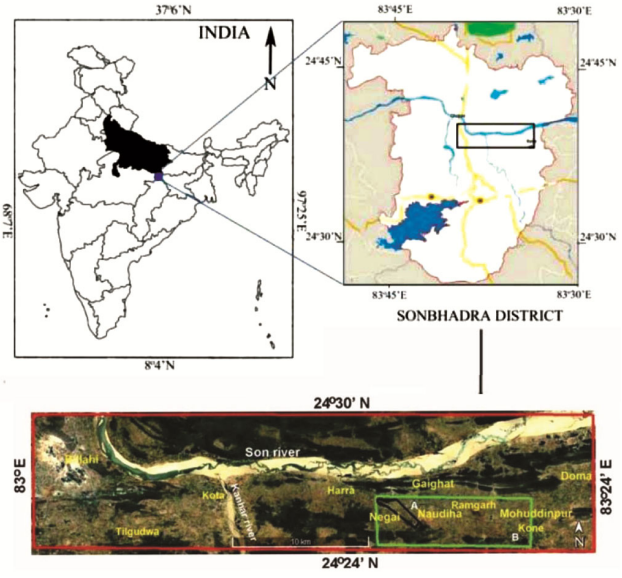

Fig. 1 — Location map of the study area[8]

Selection reasons for the use of Landsat images were their superiority[23] because of high-quality over other multispectral images such as ASTER (Advanced Space borne Thermal Emission and Reflection Radiometer) in terms of image availability during cloud-free and low humidity periods, wide scene coverage, with minor changes in the image centre location. The Area of Interest (AOI) of the study area was extracted from the downloaded satellite image and unsupervised classification was carried out using ERDAS IMAGINE 2014 software. The classifications were checked and after this stage, recoding of the colour codes as per the features was done meticulously. In this study, image was classified into nine major classes; Wastelands, Forest, Agriculture, Vegetation, Water bodies, Built-up, Kaolin, Sand, and Rocky land.

ERDAS IMAGINE 2014 was used to determine the area coverage of the study. Accuracy assessment was done in terms of user accuracy, producer accuracy, overall accuracy and Kappa Coefficient. About 256 random points were created and the minimum allowance distance was set at 30 m for each class. They were measured using Eqs 1–3.[(23)]

$$User\ Accuracy = \frac{number\ of\ correct\ points\ (value)}{The\ row\ total\ (value)} \times 100 \quad \ldots (1)$$

Producer accuracy was measured using Eq. (2)[(23)]

$$Producer\ Accuracy = \frac{Number\ of\ correct\ points\ (value)}{The\ coloumn\ total\ (value)} \times 100 \quad \ldots (2)$$

Overall accuracy was measured using Eq. (3):

$$Overall\ Accuracy = \frac{Number\ of\ total\ correct\ points\ (value)}{The\ number\ of\ points\ (value)} \times 100 \quad \ldots (3)$$

The Kappa Coefficient, K is used as a measure of agreement between model predictions and reality[24] or to ascertain if the values comprised in an error matrix represent a result significantly better than random.[25] The applied Kappa coefficients were calculated using Eq. (4):[(23,24)]

$$K = \frac{N\sum_{i=1}^{r} x_{ij} - \sum_{i=1}^{r}(x_i \times x_j)}{N^2 - \sum_{i=1}^{r}(x_i \times x_j)} \times 100 \quad \ldots (4)$$

where, N = total number of observations in matrix, xij = number of observations in row i, column j, xi = total number of observations in row i, xj =

Table 1 — Satellite details for imagery of the study area

Sl. No.	Satellite	Sensor	Spectral Bands	Month/Yearof Acquisition	Path/Row	Av.CloudCover (%)
1	Landsat 8	OLI/TIRS	11	24.02.2018	142/43	1

number of observations in column j and r = number of rows in the error matrix.

Accuracy assessment is a valuable step in the processing of remote sensing data. The actuality of the resulting data to a user is established by reference or 'ground truthing' data to support.[26] Producer's accuracy measures errors of omission that how well the real-world land cover types can be classified and the user's accuracy defines the errors in representing the likelihood of spectral information matching the land cover type of its corresponding real-world location. The overall accuracy of the classified image depends on how comparable each of its pixels is to those in the demonstrated land cover established from their ground truth data.[24,27,28]

An image classification is not complete unless its accuracy has been assessed. To ascertain the correctness, a sample of testing pixels from the categorized images is chosen, and their class identification is compared with the reference data (ground truth). The choice of a suitable sampling scheme and the determination of an appropriate sample size for testing data play a key role in the assessment of classification accuracy.[29] Overall accuracy is a standard criterion which is used to assess the accuracy of the classifications and is defined as the total number of correctly classified pixels divided by the sum of the reference pixels.[30]

Selection of sample locations and collection

Using the existing maps of the study area of Ramgarh-Naudiha, Sonbhadra district in Uttar Pradesh, and the Landsat 8 images of 2018, and the classified images generated, the sampling sites were selected.[8] The clay rich zones in the study area are marked in the digital photographs (Fig. 2).

Field survey was carried out to collect field data at various locations and 15 clay samples were collected for XRD analysis and determination of chemical and physical properties to ascertain the quality of the clays. The dried samples were ground with mortar and pestle so that the particles are finer than 0.062 mm which is small enough to avoid individual mineral separation.[8]

Identification of Clay minerals by X-ray diffraction

The most common technique to study the characteristics of crystalline structure is X-ray powder diffraction, and to determine the mineralogy of fine sediments like clays, was used in the present study. X-ray diffraction (XRD) patterns of the raw clays were recorded between the 2θ range of 10–70° with a step size of 0.02° using a Philips X'pert PRO X-Ray diffractometer (Almelo, The Netherlands) using Ni-filtered Cu-Kα radiation of wavelength 1.5406 Å. Using the Braggs equation, diffraction angle degree two theta was converted in to interplanar spacing in angstrom.

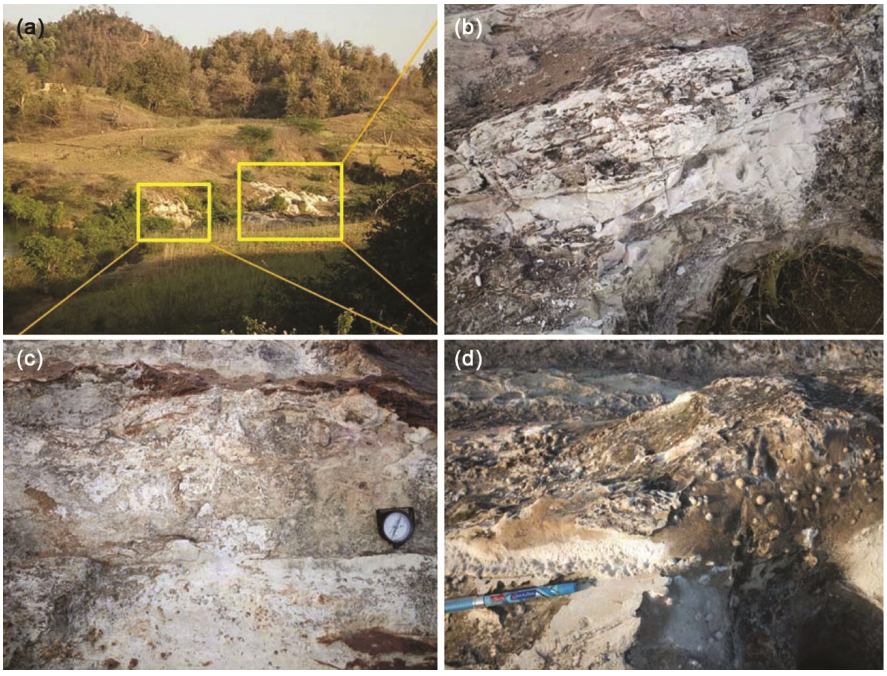

Fig. 2 — (a) Location of clay deposits in the study area, (b) and (c) are two locations with clay deposits and (d) Clay zone showing spherical calcareous noodles

$$D = \frac{\lambda_o}{2\times\sin\theta} \quad \ldots (5)$$

where,
D = Inter planer spacing in angstroms
λ = Wavelength of the characteristic X-ray
θ = X-ray diffraction angle (Bragg angle)

Chemical analysis

The chemical analysis of the -100 mesh clay material was carried out as per the methods given in the IS:4589-2002[31] standard for wet chemical analysis of ceramic whiteware clays. The alkali oxides like Na_2O and K_2O were determined by the Flame photometry.[32,33] The physical appearance of the crude mineral indicated the presence of clay with coloured minerals, soluble salts and scattered organic matter impurities.

Particle size distribution

Andreasen pipette method of particle size determination is based on Stoke's law of sedimentation. It was employed to estimate the particle size range of the clays. In a mechanical shaker, the clay was mixed with water that contained sodium pyrophosphate as a deflocculant, after which it was poured into a graduated cylinder for undisturbed settling. Without disrupting the suspension, a defined volume of the suspension was removed at predetermined time intervals, dried (110°C) in an air oven, and precisely determined their weights. The fine clay fractions collected in petridishes was dried and weighed to determine the size distribution using the Stoke's law.

Results and Discussion

Image classification Unsupervised Algorithm

The study area satellite image which has been subjected to Unsupervised classification (Fig. 3) showed nine major classes; Wastelands, Forest, Agriculture, Vegetation, Water bodies, Built-up, Kaolin, Sand, and Rocky land. The distribution table indicates that the Wasteland and Forest cover are 40.39 and 34.21% respectively. Vegetation is sporadic (9.61%) and the Water body is 4.78%. The formations like Sand, Limestone, Kaolin and Rocky land are estimated to be 4.58, 2.55, 1.08 and 0.14% respectively. The urban development in the area is as low as 2.64% as reported earlier.[22] Using ERDAS IMAGINE 2014 software, area coverage data was calculated (Table 2).

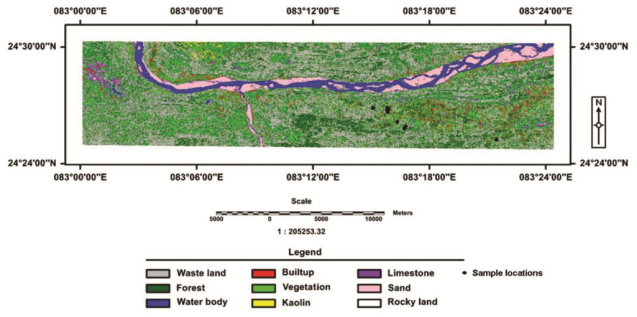

Fig. 3 — Satellite image of the study area (Unsupervised classification)

Clay sample collection spots are shown in an enlarged view of the satellite image of the study area (Fig. 4). The figure clearly shows that the clay rich zones are in the yellow coloured spots of the study area, thus giving more sources of clays.[22]

Accuracy Assessment

It is frequently necessary to support accuracy assessment for remote sensing categorisation using reference or "ground truthing" data. Making the accuracy assessment using "traditional" methods-which usually involves collecting reference data simultaneously while doing change detection using

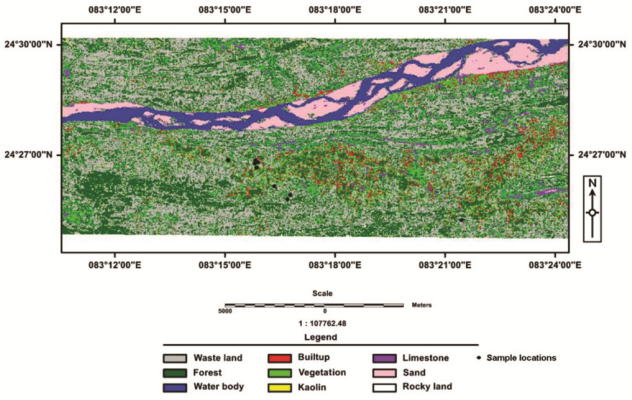

Fig. 4 — Enlarged view of the satellite image of the study area showing locations of clay samples collected as explained in the legend

Table 2 — Area coverage of the unsupervised classification

	Area (ha)	%
Waste land	16511.00	40.39
Forest	13986.10	34.21
Vegetation	3927.96	9.61
Water body	1955.56	4.78
Sand	1874.27	4.58
Built-up	1080.46	2.64
Limestone	1042.43	2.55
Kaolin	441.02	1.08
Rocky land	60.56	0.14
40879.36		

several multi-temporal images-is often challenging. This study suggests a novel strategy that argues for change rationality with post-classification comparison, as indicated in Table 3.

Using Eqs 1–4 the accuracy of each kind was computed, including wastelands, forests, agriculture, vegetation, water bodies, built-up areas, kaolin, sand, and rocky land.[22]

In Table 2, comparison of the estimated data coverage regions of the study area's classes from the 2018 Landsat picture with the accuracy assessment of the data derived from Table 4 is given.

With errors within allowable bounds, the accuracy evaluation of the 2018 computed data is accurate (Table 5). The study area is extremely exposed to natural disasters because of its location. The image analysis has helped to locate clay zones with considerable accuracy as reported.[22]

Chemical Analysis

The chemical analyses of the clay samples as given in Table 6 showed that they are quite siliceous in nature along with the presence of few other impurities. The main constituents like, SiO_2 in the range of 67–88% was mostly due to presence of free silica. Al_2O_3 content was in the range of 8–20% and Loss on Ignition (LOI) was in the 2–6.1% range.[8]

It can be seen that clay samples 31, 35A and 35B are slightly better and sample 61 is the worst in terms of composition. Presence of calcareous nodules can also be noted in the clays, which were carried by the transporting water from the adjoining limestone rich areas.

Particle sizes in clay samples and its distribution as obtained by the Andreasen pipette method using Stoke's law of sedimentation is displayed graphically (Fig. 5). The industry requirements clearly indicate that the Grade I and Grade III clays must contain at least 70 and 45% sub 2 μm fractions respectively. However, our best clay sample 35B picked up from the study area is dominated with (~45%) 8 μm size with only 30% sub 2 μm fraction.

The worst clay specimen picked up (61) had almost linearly decreasing content of finer clay fraction in the 25 to 2 micron range. So, the best clays collected in the study area do not qualify the ceramic industry requirements in terms of particle size distribution, and as a result, plasticity. Lower manufacturing costs could result by partially substituting the relatively expensive fine clays in the ceramic industry with the clay deposits under investigation.

Table 4 — Producers accuracy and users accuracy

Class Name	Producers accuracy (%)	Users accuracy (%)
Waste land	90.82	86.41
Forest	96.10	84.09
Water body	71.43	83.33
Built-up	54.55	85.71
Vegetation	70.97	91.67
Kaolin	60.00	99.98
Limestone	100.00	85.71
Sand	85.71	99.99
Rocky land	—	—

Table 5 — Overall kappa statistics

Overall Kappa Statistics = 0.8166

Kappa estimated for each Category

Class Name	Kappa
Waste land	0.78
Forest	0.77
Water body	0.82
Built-up	0.85
Vegetation	0.91
Kaolin	0.99
Limestone	0.85
Sand	0.99
Rocky land	0

Table 3 — Accuracy Assessment of the classification

Classified Data	Waste land	Forest	Water Body	Built-up	Vegetation	Kaolin	Limestone	Sand	Rocky land	Row Total
Waste land	**89**	3	3	3	5	0	0	0	0	103
Forest	6	**74**	1	1	4	2	0	0	0	88
Water body	1	0	**10**	0	0	0	0	1	0	12
Built-up	0	0	0	**6**	0	0	0	1	0	7
Vegetation	2	0	0	0	**22**	0	0	0	0	24
Kaolin	0	0	0	0	0	**3**	0	0	0	3
Limestone	0	0	0	1	0	0	**6**	0	0	7
Sand	0	0	0	0	0	0	0	**12**	0	12
Rocky land	0	0	0	0	0	0	0	0	0	0
Column Total	98	77	14	11	31	5	6	14	0	**256**

Table 6 — Chemical analysis of raw Clay Samples

Sample Nos.	1	2	3	4	5	6	7	8	9	10	11	12	13	14	15
	Sample reference														
Constituents (%)	**31**	**32A**	**32B**	**33A**	**33B**	**35A**	**35B**	**36**	**37A**	**37B**	**37C**	**40A**	**40B**	**40C**	**61**
SiO_2	69.31	71.08	71.01	72.00	72.35	67.33	67.50	86.55	80.87	80.84	78.97	75.37	75.53	77.17	87.67
Al_2O_3	17.46	16.06	16.26	17.32	17.17	19.81	19.74	8.70	10.54	10.33	12.30	15.64	17.38	15.54	8.10
Fe_2O_3	1.40	1.46	1.40	1.74	1.56	2.02	1.98	0.80	1.25	1.34	0.96	0.52	0.31	0.40	0.10
TiO_2	0.27	0.47	0.37	0.62	0.54	0.67	0.56	0.33	0.32	0.30	0.34	0.30	0.17	0.20	0.15
CaO	1.04	0.35	0.30	0.35	0.32	0.07	0.02	0.34	0.70	0.62	0.52	1.74	0.41	0.67	0.22
MgO	0.86	4.57	4.86	1.80	1.67	1.94	1.96	0.59	1.75	1.77	0.49	0.08	0.29	0.40	0.62
Na_2O	0.58	0.67	0.58	0.42	0.44	0.27	0.35	0.34	0.23	0.26	0.58	0.33	0.20	0.21	0.31
K_2O	2.97	0.15	0.11	0.19	0.15	1.95	1.97	0.20	0.89	0.83	1.56	1.10	0.71	0.48	0.19
LOI	6.01	5.09	5.01	5.47	5.75	5.88	5.89	2.07	3.39	3.60	4.18	4.88	4.92	4.89	2.55

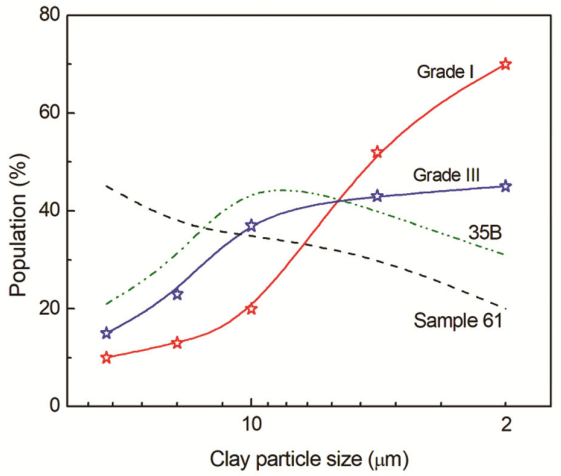

Fig. 5 — Population (%) of clay fraction versus particle size for two selected samples collected from the study area in the Ramgarh-Naudiha region of Sonbhadra district along with Grade I and Grade III china clays used in ceramic industries

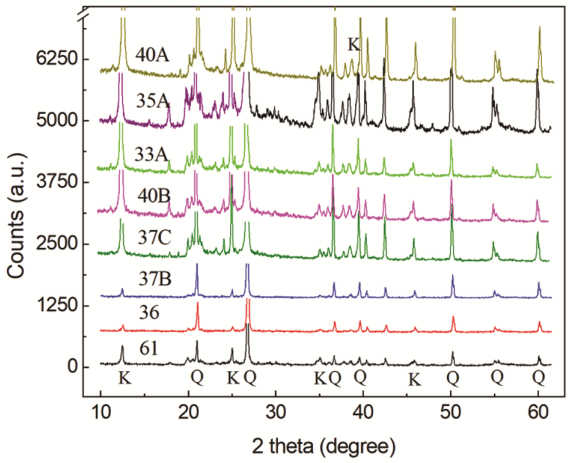

Fig. 6 — X-ray diffraction (XRD) patterns of some of the clay samples collected from the study area;[8] The layers in the Y-axis (intensity values) are scaled to avoid overlapping

X-Ray Diffraction

Graphs plotted as X-ray peaks versus diffraction angle 2θ are the X-ray diffraction (XRD) patterns of the representative raw clay samples that were obtained from the Ramgarh-Naudiha area of the Sonbhadra district (Fig. 6).

The occurrence of (100) and (101) peaks of low quartz at 20.5 and 26.66° 2θ, respectively, indicates that the minerals mostly contain linked siliceous impurities in the unwashed clay (ICDD card 5-490). Mica, feldspar, and quartz are the related mineral impurities found in the raw clay, as proved by X-ray patterns on careful observation. The presence of X-ray peaks from (001), (002), and {(202), (131)} planes at 12.4, 24.94, and 38.5 degree two theta verified that the weakly crystallised kaolinite (ball clay) contributed to the clay's workability (ICDD card 5-143). The higher Fe_2O_3 and TiO_2 contents contribute an ivory to buff colour which on firing at temperatures above 800°C produces white burnt china clay.

Conclusions

The characteristics of the clay deposits, which are ball clays, suggest that they may have originated from the weathering and decomposition of granitic rocks before being carried and deposited into the surrounding basin by the flowing river. The clay's fine-grained texture is resulted from the particle-particle attrition during the flow process. Ball clays require more water than typical china clays. Nodules that had been eroded from the surrounding limestone deposits are visible in the outcrops of the clay deposit. These clays have a higher SiO_2 content as a result of silica from the surrounding areas. Raw ball clays are

light brown to almost black depending on the amount of organic matter content. The study finds that remote sensing techniques can be used to efficiently map the geographical distribution of mineral deposits, which can significantly save cost, time, and resources when compared to conventional methods of mineral mapping. Remote sensing can be used all over the country to map newer or relatively smaller sources of different minerals. This map should be validated by ground-truth data by field surveys which will enhance the clay mineral resources of the country.

Acknowledgements

The authors are extremely thankful to Director, CSIR-Central Glass & Ceramic Research Institute for permitting the study and using its laboratory facilities. Technical staffs helped the testing of samples. The Geology Department, Aligarh Muslim University, provided facilities for carrying out the XRD analysis. Thanks are also to the Directorate of Geology and Mining, Government of Uttar Pradesh for giving important guidance about the clay deposits in the area. We are thankful to AIGIRS, Noida for facilities provided and advise in preparation of this article.

References

1 Farina P, Catani F, Colombo D, Fumagalli A, Kukavicic M, Marks F & Moretti S, Remote sensing: a tool for landslide investigations at a basin scale, *Geophys Res Abs*, **7** (2005) 10157–10168.

2 Akbari E, Amiri N & Azizi H, Remote sensing and land use extraction for kernel functions analysis by support vector machines with ASTER multispectral imagery, *Iran J Earth Sci*, **4** (2012) 85–94.

3 Aminzadeh B & Samani F, Identifying the boundaries of the historical site of Persepolis using remote sensing, *Remote Sens Environ*, **102** (2006) 52–62, https://doi.org/10.1016/j.rse.2006.01.018.

4 Hunt G R, Spectral signatures of particulate minerals in the visible and near infrared, *Geophys*, **42** (1977) 501–513, https://doi.org/10.1190/1.1440721.

5 Kruse F A, Perry S L & Caballero A, District-level mineral survey using airborne hyperspectral data, Los Menucos, Argentina, *Ann Geophys Italy*, (2006) 49, https://doi.org/10.4401/ag-3154.

6 Khodami M & Kamali Shervedani A, Mineralogical and geochemical characteristics of the Chah-Shur clay deposit, Southeast of Isfahan, Iran, *Iran J Earth Sci*, **10** (2018) 135–141.

7 Fakhari S, Jafarirad A, Afzal P & Lotfi M, Delineation of hydrothermal alteration zones for porphyry systems utilizing ASTER data in Jebal-Barez area, SE Iran, *Iran J Earth Sci*, **11** (2019) 80–92, https://doi.org/10.30495/ijes.2019.664780.

8 Karmakar D, Singh V, Veerabhadrappa S M, Singh R, Sharma L K & Ghosh S, Beneficiation of Clays from Ramgarh- Naudiha Region of Sonbhadra District Uttar Pradesh, Impart Improved Properties for Ceramic Industries, *Indian J Eng Mater Sci*, **30** (2023) 65–72, https://doi.org/10.56042/ijems.v1i1.64836.

9 Santamaría-López Á, Suárez M & García-Romero E, Detection limits of kaolinites and some common minerals in binary mixtures by short-wave infrared spectroscopy, *Appl Clay Sci*, **250** (2024) 107269, https://doi.org/10.1016/j.clay.2024.107269.

10 Vie R, Azema N, Quantin J, Touraud E & Fouletier M, Study of suspension settling: A approach to determine suspension classification and particle interactions, *Colloid Surface A,* **298** (2007) 192–200, https://doi.org/10.1016/j.colsurfa.2006.10.074.

11 Teh E-J, Leong Y-K, Liu Y, Fourie A & Fahey M, Differences in the rheology and surface chemistry of kaolin clay slurries: The source of the variations, *Chem Eng Sci*, **64** (2009) 3817–3825, https://doi.org/10.1016/j.ces.2009.05.015.

12 Gupta V, Hampton M A, Stokes J R, Nguyen A V & Miller J D, Particle interactions in kaolinite suspensions and corresponding aggregate structures, *J Colloid Interf Sci*, **359** (2011) 95–103, https://doi.org/10.1016/j.jcis.2011.03.043.

13 Awad M E, López-Galindo A, Setti M, El-Rahmany M M & Iborra C V, Kaolinite in pharmaceutics and biomedicine, *Int J Pharm,* **533** (2017) 34–48, https://doi.org/10.1016/j.ijpharm.2017.09.056.

14 Ptáček P, Opravil T, Šoukal F, Wasserbauer J, Másilko J & Baráček J, The influence of structure order on the kinetics of dehydroxylation of kaolinite, *J Eur Ceram Soc*, **33** (2013) 2793–2799, https://doi.org/10.1016/j.jeurceramsoc.2013.04.033.

15 Wardhana Y W, Hasanah A & Primandini P, Deformation and adsorption capacity of kaolin that is influenced by temperature variation on calcination, *Int J Pharm Pharm Sci*, **6** (2014) 1–2.

16 Ndlovu B, Farrokhpay S, Forbes E & Bradshaw D, Characterisation of kaolinite colloidal and flow behaviour via crystallinity measurements, *Powder Technol*, **269** (2015) 505–512, https://doi.org/10.1016/j.powtec.2014.09.029.

17 Ben-Dor E, Irons J R, Epema G F, Soil reflectance, in *Remote Sensing for the Earth Sciences: Manual of Remote Sensing*, edited by N Rencz, (John Wiley & Sons, New York) 1999, 111–188.

18 Dogan H, Applications of remote sensing and Geographic Information Systems to assess ferrous minerals and iron oxide of Tokat province in Turkey, *Int J Remote Sens*, **29** (2008) 221–233, https://doi.org/10.1080/01431160701269010.

19 Dogan H M, Mineral composite assessment of Kelkit River Basin in Turkey by means of remote sensing, *J Earth Syst Sci*, **118** (2009) 701–710.

20 Rajesh, H M, Application of remote sensing and GIS in mineral resource mapping-An overview, *J Miner Petrol Sci*, **99** (2004), 83–103, https://doi.org/10.2465/jmps.99.83.

21 Sikakwe, G U, Mineral exploration employing drones, contemporary geological satellite remote sensing and geographical information system (GIS) procedures: A review, *Remote Sens Appl*, **31** (2023) 100988, https://doi.org/https://doi.org/10.1016/j.rsase.2023.100988.

22 Karmakar D, Singh V, Singh R, Sharma L K & Ghosh, S, Land Use/Land Cover Change and Environmental Impact Analysis of Ramgarh-Naudiha Region in Uttar Pradesh, India

through Geospatial Technology, *J Sci Ind Res*, **82** (2023) 475–484, https://doi.org/10.56042/jsir.v82i04.70789.

23 Tilahun A & Teferie B, Accuracy assessment of land use land cover classification using Google Earth, *Am J Environ Prot*, **4** (2015) 193–198, https://doi.org/10.11648/j.ajep.20150404.14.

24 Congalton R G, A review of assessing the accuracy of classifications of remotely sensed data, *Remote Sens Environ*, **37** (1991) 35–46, https://doi.org/10.1016/0034-4257(91)90048-B.

25 Jensen J R & Cowen D C, Remote sensing of urban/suburban infrastructure and socio-economic attributes, *Photogramm Eng Remote Sens*, **65** (1999) 611–622.

26 Fung T & LeDrew E, For change detection using various accuracy, *Photogramm Eng Remote Sens*, **54** (1988) 1449–1454, https://doi.org/10.1016/0034-4257(95)00233-2.

27 Unger H & Tanya S, Introductory digital image processing: A remote sensing perspective, (2007) 89–90, https://doi.org/10.2113/gseegeosci.13.1.89.

28 Rwanga S S & Ndambuki J M, Accuracy assessment of land use/land cover classification using remote sensing and GIS, *Int J Geosci*, **8** (2017) 611, https://doi.org/10.4236/ijg.2017.84033.

29 Chakravarty S, Ghosh S, Suresh C, Dey A & Shukla G, Deforestation: Causes, effects and control strategies, *Global Perspectives on Sustainable Forest Management*, **1** (2012) 1–26, https://doi.org/10.5772/33342.

30 Mallupattu P K & Reddy S J R, Analysis of land use/land cover changes using remote sensing data and GIS at an urban area, Tirupati, India, *The Sci World J*, **1** (2013) 268623, https://doi.org/10.1155/2013/268623.

31 Indian Standards, Specification, Plastic clay and washed plastic clay for ceramic industry, IS:4589 (2002).

32 Sen S, Beneficiation of China clay, *T Indian Ceram Soc*, **23** (1964) 1–6, https://doi.org/10.1080/0371750X.1964.10855473.

33 Sen S & Guha S, Quality of Indian clays and their improvement, *T Indian Ceram Soc*, **27** (1968) 19N–23N, https://doi.org/10.1080/0371750X.1968.10855661.